

# Denoising via Repainting: an image denoising method using layer wise medical image repainting

Arghya Pal, Sailaja Rajanala, CheeMing Ting, Raphael Phan

Monash University  
arghya.pal@monash.edu

**Abstract.** Medical image denoising is essential for improving the reliability of clinical diagnosis and guiding subsequent image-based tasks. In this paper, we propose a multi-scale approach that integrates anisotropic Gaussian filtering with progressive Bezier-path redrawing. Our method constructs a scale-space pyramid to mitigate noise while preserving critical structural details. Starting at the coarsest scale, we segment partially denoised images into coherent components and redraw each using a parametric Bezier path with representative color. Through iterative refinements at finer scales, small and intricate structures are accurately reconstructed, while large homogeneous regions remain robustly smoothed. We employ both mean square error and self-intersection constraints to maintain shape coherence during path optimization. Empirical results on multiple MRI datasets demonstrate consistent improvements in PSNR and SSIM over competing methods. This coarse-to-fine framework offers a robust, data-efficient solution for cross-domain denoising, reinforcing its potential clinical utility and versatility. Future work extends this technique to three-dimensional data.

**Keywords:** Denoising, Multi-scale, Anisotropic Filtering, Bezier Paths, MRI.

## 1 Introduction

Denoising is a fundamental challenge in MRI, with applications ranging from surgical planning to diagnostic interpretation. While conventional approaches (e.g., wavelet thresholding, nonlocal means) and unsupervised or self-supervised strategies (e.g., Aniso [9], nonlocal [3], Beltrami [2]) have shown promise for reducing high-frequency noise, they often struggle to maintain fine structures and subtle details critical for clinical decision-making. Recent advances in deep learning DnCNN [11], N2N [7], Ne2Ne [4]) have demonstrated significant improvements in reconstruction quality by learning end-to-end mappings between noisy inputs and clean targets. However, these learned models typically require extensive labeled data and may not generalize well to unseen noise distributions or different imaging modalities.

In this work, we propose a novel denoising framework that integrates *multi-scale anisotropic filtering* and a *progressive component-redrawing* strategy to

robustly mitigate noise in diverse medical images. As illustrated in Fig. 1 (top), our method first constructs an *anisotropic Gaussian blur pyramid* (i.e., a scale space) to incrementally isolate noise from salient anatomical features. Beginning with a heavily smoothed representation and progressing to finer scales, we adaptively preserve edges, corners, and textural patterns across modalities. We then segment each partially denoised image into coherent regions and redraw these regions using parametric Bézier paths, thereby maintaining the structural integrity of the underlying tissue boundaries. This coarse-to-fine redrawing strategy ensures that large homogeneous regions are captured early, while smaller or more complex structures are refined in subsequent iterations.

Compared to purely data-driven solutions, our method does not require extensive labeled training data, as it inherently incorporates spatial continuity constraints through anisotropic smoothing. Moreover, the proposed formulation accommodates multiple noise levels without additional retraining, making it especially suitable for real-world clinical scenarios where noise characteristics can vary widely. Experimental results on multiple MRI datasets, including AxFLAIR brain MRI and Cor-PD knee MRI, demonstrate that our approach consistently achieves state-of-the-art performance in terms of both PSNR and SSIM, while also retaining critical anatomic details. By effectively balancing noise reduction and structure preservation, the presented framework broadens the applicability of denoising methods to a wide range of medical imaging applications.

## 2 Methodology

Our proposed approach is designed to denoise a given image by leveraging a multi-scale, anisotropic Gaussian blur pyramid (i.e., a scale space), followed by progressive component identification and redrawing. As shown in Fig. 1 (top), the denoising is carried out in a coarse-to-fine manner by incrementally adding Bezier paths that represent image components with coherent color and texture. We detail each step below.

### 2.1 Step 1: Scale-Space Pyramid

We begin with the assumption that no prior knowledge of the noise distribution is available. Hence, the core objective of this step is to isolate essential image structures (e.g., edges, corners) from unstructured high-frequency noise. To achieve this, we construct an *anisotropic Gaussian blur* scale-space pyramid, motivated by the principles in [9].

*Anisotropic Gaussian Blur.* Let  $I$  be the original noisy image. We define the  $t$ -th scale-space image  $I_t$  by:

$$I_t = G(\mu_t, \sigma_t) * I + \nabla I + \Delta I, \quad t = 0, \dots, T, \quad (1)$$

where  $G(\mu_t, \sigma_t)$  is an anisotropic Gaussian kernel parameterized by  $\mu_t$  and  $\sigma_t$ . By varying these parameters from large (producing a strongly blurred image)

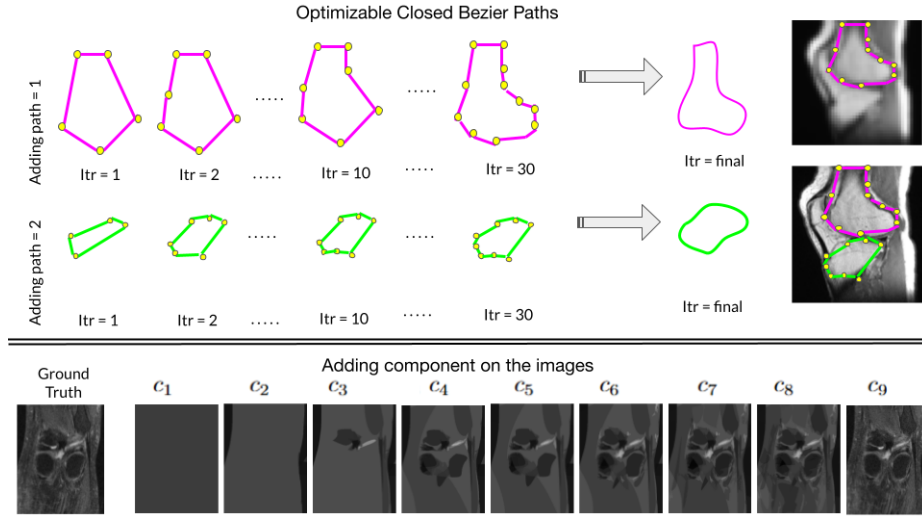


**Fig. 1.** (Top) Our methodology (§2) progressively adds Bezier paths for each component in a coarse-to-fine manner. (Bottom) Demonstration of denoising an image in a layer-wise coarse-to-fine manner with redrawing using a small number of paths.  $c_1, \dots, c_9$  indicate the path numbers.

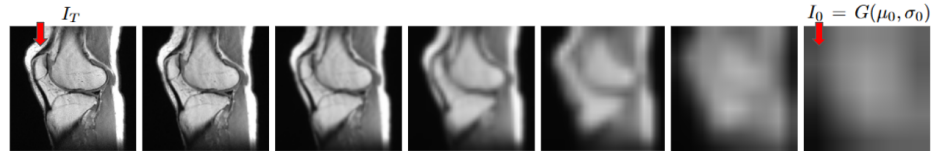


**Fig. 2.** Anisotropic Gaussian Blur with varying  $G(\mu_t, \sigma_t)$  [9]. Larger values of  $\mu_t$  and  $\sigma_t$  yield stronger smoothing, while smaller values preserve finer details.

to small (retaining finer details), we obtain multiple scales of smoothing. The operators  $\nabla I$  and  $\Delta I$  represent the gradient and Laplacian of the noisy image  $I$ , respectively.

*Scale-Space Construction.* We form a sequence of images  $\{I_0, I_1, \dots, I_T\}$ , each providing a different trade-off between noise suppression and edge preservation:

- Larger  $\sigma_t$  and  $\mu_t$  values favor stronger smoothing to eliminate high-frequency noise.
- Smaller  $\sigma_t$  and  $\mu_t$  values preserve detailed structures (e.g., edges, corners).

Figure 2 illustrates the impact of varying  $(\mu_t, \sigma_t)$ . In practice,  $I_0$  (the first level) is often the most heavily smoothed image and serves as the basis for subsequent redrawing.

## 2.2 Step 2: Progressive Component Redrawing in $I_0$

Once we obtain  $I_0$ , a partially denoised and smoothed image, we segment it into connected components  $\{c_1, \dots, c_N\}$  based on color or texture continuity. The assumption is that spatially contiguous pixels with similar color attributes can be grouped into coherent regions, each corresponding to a uniform color/texture area.

*Bezier-Path Representation.* For each component  $c_n$ , we redraw its shape and color using a parameterized Bezier path (Fig. 1, top). We represent each component as a sequence of  $k$  cubic Bézier segments, where each segment  $i$  is defined by control points  $\{\mathbf{P}_{i,j}\}_{j=0}^k$  and parameterized for  $j \in [0, 1]$  by

$$\mathbf{B}_i(t) = (1-t)^3 \mathbf{P}_{i,0} + 3t(1-t)^2 \mathbf{P}_{i,1} + 3t^2(1-t) \mathbf{P}_{i,2} + t^3 \mathbf{P}_{i,3}.$$

To ensure these segments form a closed loop, we impose the positional continuity constraints

$$\mathbf{P}_{i,3} = \mathbf{P}_{(i+1) \bmod n, 0} \quad \text{for } i = 0, \dots, n-1,$$

This path captures the topological outline of the component and assigns a representative color derived from  $I_0$ . Following [8], we employ an  $l_1$ -based color difference metric to check the fidelity of the redrawn region compared to the partially denoised image:

$$\text{Diff}(c_n, I_0) = \|c_n^{(\text{redrawn})} - c_n^{(I_0)}\|_1.$$

If this discrepancy is below a predefined threshold (e.g., 0.1), the component is accepted. Otherwise, the Bezier path is refined, or a new initialization is considered.

## 2.3 Step 3: Iteration & Optimization Across Scales

We refine the denoising at multiple resolutions by repeating the redrawing procedure for the subsequent images  $I_1, I_2, \dots, I_T$  in the scale-space pyramid. Specifically:

1. **Identify New Components at Scale  $I_t$ .** Additional or refined structures not visible at  $I_{t-1}$  emerge, denoted  $\{c_{N+1}, \dots, c_{N+M}\}$ .
2. **Add/Refine Bezier Paths.** We introduce new Bezier paths for newly identified components  $\{c_{N+1}, \dots, c_{N+M}\}$  and may increase control points in previously identified paths to improve boundary accuracy.
3. **Update Reconstructed Image.** By overlaying each newly rendered or refined component, the image is incrementally “painted” in a coarse-to-fine manner.

Figure 1 (bottom) showcases how each new component addition helps to fill in critical details while mitigating noise. Larger regions (e.g., background) are captured first at coarser scales, while finer structures (e.g., edges, tissue boundaries) are accurately detailed at higher-resolution scales. This iterative strategy balances noise reduction with preserving essential image topology and color continuity. We represent the methodology in Algorithm 1.

---

**Algorithm 1:** Proposed Multi-Scale Anisotropic Rendering

---

**Input:** Noisy image  $I$ ,  
Number of scale-space levels  $T$ ,  
Learning rates  $\alpha, \beta$ ,  
Regularization weight  $\lambda$ ,  
Iterations per scale level  $t_{\max}$   
**Output:** Denoised Image

**Step 1: Build Scale-Space Pyramid (Sec. 2.1)**  
Construct  $\{I_0, \dots, I_T\}$  via anisotropic Gaussian blur at multiple scales.

**Step 2: Initialization at Coarsest Scale (Sec. 2.2)**  
Identify initial components in  $I_0$ , initialize their Bezier-path control points  $\mathbf{P}$  and colors  $\mathbf{C}$ .

**Step 3: Optimize Paths at Coarsest Scale (Sec. 2.2)**  
**for**  $j = 1$  **to**  $t_{\max}$  **do** // Gradient-descent loop  
    Render image  $\hat{I}_0$  from  $\mathbf{P}, \mathbf{C}$ .  
    Compute MSE and Xing-loss [8] (cf. Sec. 2.3).  
    Update  $\mathbf{P}$  and  $\mathbf{C}$  using learning rates  $\alpha, \beta$ .  
Update the pixel-wise loss weight based on the final MSE.

**Step 4: Iterative Refinement Across Scales (Sec. 2.3)**  
**for**  $t = 1$  **to**  $T$  **do** // From finer scales  $I_1$  to  $I_T$   
    Identify or refine new components at scale  $I_t$ .  
    Append new paths/colors  $\mathbf{P}, \mathbf{C}$  for these components.  
    **for**  $j = 1$  **to**  $t_{\max}$  **do**  
        Render  $\hat{I}_t$ .  
        Compute MSE and Xing-loss (Sec. 2.3).  
        Update  $\mathbf{P}, \mathbf{C}$  via gradient descent.  
    Update pixel-wise loss weight based on MSE at scale  $I_t$ .

**return** *Final Denoised Image*  $\{\mathbf{P}, \mathbf{C}\}$  // Denoised representation

---

## 2.4 Step 4: Loss Functions

A commonly used loss function to measure the discrepancy between the noisy image  $I \in \mathbb{R}^{w \times h \times 3}$  and a rendered output  $\hat{I}_t \in \mathbb{R}^{w \times h \times 3}$  is the *mean square error (MSE)*. Despite its simplicity, MSE remains effective for many image comparison and reconstruction tasks because it is straightforward to implement and computationally efficient. It is possible for some Bezier Paths to become self-interacted during the course of optimization, leading to detrimental artifacts and improper topology. To this end, we adopt the self interaction Xing-loss [8] to mitigate this problem. Assuming all the Bezier curves in our paper are third order, by analyzing a number of optimized shapes, the [8] found that a self-interacted path always intersects the lines of its control points, and vice versa. This suggests that instead of optimizing the Bezier path, one potential solution would be adding a constraint on the control points.

**Table 1.** Quantitative comparison of DnCNN, N2N, N2void, Ne2Ne, Restoformer, LAN, Anisotropic, nonlocal, Beltrami, and our method. We report PSNR (dB) / SSIM. “-” indicates no result was provided.

Model	Method	$\sigma$	PSNR/SSIM	PSNR/SSIM	PSNR/SSIM	PSNR/SSIM
			AxFLAIR	Cor-PD knee	FastMRI Breast	FastMRI Prostate
<b>Training</b>	DnCNN [11]	-	38.10/0.952	-	36.60/0.930	-
		5	38.07/0.951	38.08/0.951	36.60/0.929	36.60/0.929
	N2N [7]	10	38.04/0.950	38.06/0.951	36.59/0.928	36.60/0.928
		20	37.99/0.949	38.02/0.949	36.56/0.925	36.56/0.925
		5	37.93/0.948	37.95/0.948	36.48/0.923	36.46/0.923
	N2void [6]	10	37.76/0.943	37.83/0.945	36.29/0.915	36.28/0.915
		20	37.47/0.935	37.67/0.941	35.95/0.902	36.02/0.904
		5	38.12/0.952	38.13/0.952	36.69/0.931	36.70/0.931
	Ne2Ne [4]	10	38.13/0.952	38.14/0.952	36.75/0.931	36.77/0.931
		20	38.13/0.952	38.14/0.952	36.78/0.930	36.81/0.930
		5	38.23/0.955	38.23/0.956	36.56/0.936	36.54/0.935
	Restoformer [10]	10	38.23/0.955	38.25/0.955	36.66/0.934	36.65/0.934
		20	38.17/0.953	38.20/0.954	35.69/0.931	36.68/0.930
		5	38.22/0.954	38.16/0.953	36.73/0.934	36.66/0.932
	LAN [5]	10	38.29/0.955	38.22/0.954	36.79/0.936	36.71/0.933
		20	38.29/0.955	38.31/0.956	36.78/0.938	36.80/0.935
		5	39.09/0.966	39.04/0.965	38.14/0.952	38.07/0.951
	<b>Untrained</b>	Anisotropic [9]	10	39.12/0.965	39.04/0.965	38.23/0.952
20			39.14/0.965	38.98/0.964	38.35/0.953	38.05/0.948
5			39.04/0.965	39.00/0.965	38.12/0.951	38.07/0.950
nonlocal [3]	10	38.96/0.964	38.89/0.964	38.05/0.950	37.95/0.948	
	20	38.74/0.961	38.66/0.961	37.65/0.943	37.52/0.941	
	5	39.07/0.965	39.08/0.965	38.09/0.951	38.10/0.951	
Beltrami [2]	10	39.06/0.965	39.07/0.965	38.12/0.950	38.14/0.950	
	20	39.02/0.964	39.03/0.964	38.12/0.948	38.14/0.948	
<b>Ours</b>	5	39.23/0.968	39.09/0.967	38.31/0.957	38.14/0.953	
	10	39.30/0.969	39.14/0.967	38.58/0.961	38.25/0.955	
	20	39.28/0.969	39.17/0.968	38.86/0.965	38.38/0.958	

### 3 Results

*Dataset.* We use AxFLAIR brain MRI, Cor-PD knee MRI, FastMRI, and Modl [1] datasets to show the efficacy of our model.

*Qualitative Comparison.* Table 1 presents a comprehensive comparison of representative denoising approaches, including both supervised (e.g., DnCNN [11], N2N [7], Ne2Ne [4]) and unsupervised or self-supervised strategies (e.g., Aniso [9], nonlocal [3], Beltrami [2]), as well as our proposed method. Performance is reported in terms of PSNR and SSIM under varying noise levels  $\sigma$  (5, 10, and 20), across four anatomical regions—Knee, Head, Breast, and Prostate. A dash (“-”) indicates that no result was available for that specific condition. Overall, the results demonstrate that our approach consistently outperforms most baseline methods on multiple tissue types, confirming its robustness and versatility in cross-domain medical image denoising.

*Qualitative Comparisons.* We show in Figs 4 and 3 to show the qualitative comparison of our images. From the enlarged view of Fig. 3, it is not difficult to find that the image reconstructed by DnCNN [11], N2N [7], Ne2Ne [4], Resto-

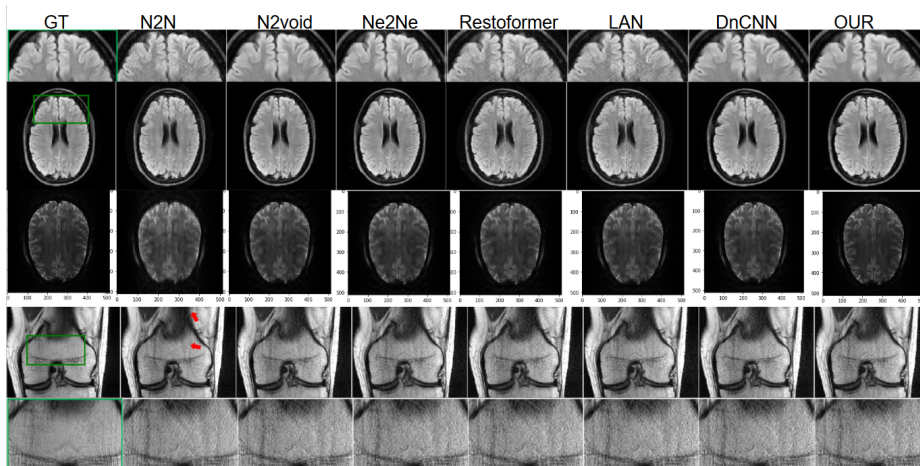


**Fig. 3.** (Top) AxFLAIR brain MRI, (Bottom) Cor-PD knee MRI; qualitative comparison of DnCNN [11], N2N [7], Ne2Ne [4], Restoformer [10], N2void [6], LAN [5], and our method. First column represent ground truth image.

former [10], N2void [6], LAN [5] methods. Fig. 3 shows the denoising results of trained models on a noise pattern  $\sigma = 15$ , see first image of the second row in Fig. 3. The experimental results are consistent with the above experimental performance, which further verifies the robustness of our method in terms of noise pattern.

## 4 Discussion and Conclusion

In this work, we introduced a multi-scale approach for denoising medical images by combining anisotropic Gaussian filtering and progressive Bezier-path redrawing. Through extensive evaluation on diverse MRI datasets (including AxFLAIR and Cor-PD knee MRI), our method demonstrates robust performance in terms of PSNR and SSIM, while preserving essential anatomical details such as tissue boundaries and subtle textural structures. A key advantage of our framework lies in its adaptability: by tuning the anisotropic blur parameters, our approach can address a wide range of noise levels without demanding extensive labeled training data.

Despite these benefits, there are some practical considerations. First, the iterative nature of the Bezier-path redrawing introduces a computational overhead, especially for high-resolution images. Approaches to accelerate convergence, such as leveraging multi-GPU or parallelized rendering strategies, could further improve usability in time-sensitive clinical settings. Second, while the anisotropic blur provides flexibility across different noise characteristics, further exploration of adaptive parameter selection (e.g., learning the blur hyperparameters) might

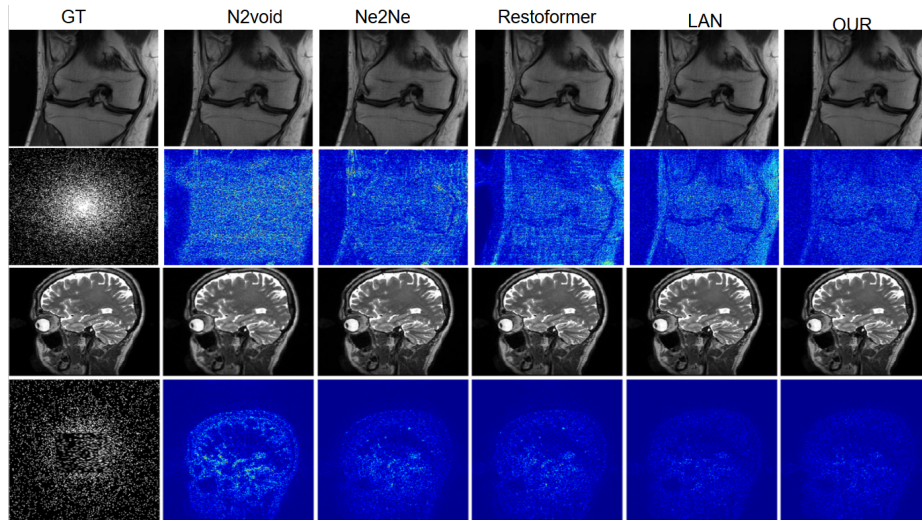


**Fig. 4.** (Top) FastMRI knee reconstruction, (Bottom) Modl [1] Brain MRI; qualitative comparison of Ne2Ne [4], Restoformer [10], N2void [6], LAN [5], and our method. First column represent ground truth image.

enhance robustness in scenarios involving highly heterogeneous noise distributions.

In conclusion, our multi-scale denoising framework addresses both low- and high-frequency noise in a principled, coarse-to-fine manner. The proposed method effectively balances shape preservation and noise suppression, outperforming many conventional and learned denoising baselines across various anatomical regions. Future work will focus on extending our approach to 3D volumetric data and exploring how semantic information (e.g., segmentation masks) may be incorporated to guide the redrawing process. We believe that these developments will pave the way for more accurate and clinically valuable image reconstructions in numerous medical imaging applications.

## References

1. Aggarwal, H.K., Jacob, M.: Model adaptation for image reconstruction using generalized stein’s unbiased risk estimator. arXiv preprint arXiv:2102.00047 (2021)
2. Ben-Loghfyry, A., Hakim, A., Laghrib, A.: A denoising model based on the fractional beltrami regularization and its numerical solution. *Journal of Applied Mathematics and Computing* **69**(2), 1431–1463 (2023)
3. Guidotti, P.: A new nonlocal nonlinear diffusion of image processing. *Journal of Differential Equations* **246**(12), 4731–4742 (2009)
4. Huang, T., Li, S., Jia, X., Lu, H., Liu, J.: Neighbor2neighbor: Self-supervised denoising from single noisy images. In: *Proceedings of the IEEE/CVF Conference on Computer Vision and Pattern Recognition (CVPR)*. pp. 14781–14790 (June 2021)

5. Kim, C., Kim, T.H., Baik, S.: LAN: Learning to Adapt Noise for Image Denoising . In: 2024 IEEE/CVF Conference on Computer Vision and Pattern Recognition (CVPR). pp. 25193–25202. IEEE Computer Society, Los Alamitos, CA, USA (Jun 2024). <https://doi.org/10.1109/CVPR52733.2024.02380>, <https://doi.ieeecomputersociety.org/10.1109/CVPR52733.2024.02380>
6. Krull, A., Buchholz, T.O., Jug, F.: Noise2void-learning denoising from single noisy images. In: Proceedings of the IEEE Conference on Computer Vision and Pattern Recognition. pp. 2129–2137 (2019)
7. Lehtinen, J., Munkberg, J., Hasselgren, J., Laine, S., Karras, T., Aittala, M., Aila, T.: Noise2Noise: Learning image restoration without clean data. In: Dy, J., Krause, A. (eds.) Proceedings of the 35th International Conference on Machine Learning. Proceedings of Machine Learning Research, vol. 80, pp. 2965–2974. PMLR (10–15 Jul 2018), <https://proceedings.mlr.press/v80/lehtinen18a.html>
8. Ma, X., Zhou, Y., Xu, X., Sun, B., Filev, V., Orlov, N., Fu, Y., Shi, H.: Towards layer-wise image vectorization. In: Proceedings of the IEEE conference on computer vision and pattern recognition (2022)
9. Perona, P., Malik, J.: Scale-space and edge detection using anisotropic diffusion. IEEE Transactions on pattern analysis and machine intelligence **12**(7), 629–639 (1990)
10. Zamir, S.W., Arora, A., Khan, S., Hayat, M., Khan, F.S., Yang, M.H.: Restormer: Efficient transformer for high-resolution image restoration. In: Proceedings of the IEEE/CVF conference on computer vision and pattern recognition. pp. 5728–5739 (2022)
11. Zhang, K., Zuo, W., Chen, Y., Meng, D., Zhang, L.: Beyond a gaussian denoiser: Residual learning of deep cnn for image denoising. IEEE Transactions on Image Processing **26**(7), 3142–3155 (2017). <https://doi.org/10.1109/TIP.2017.2662206>